REPORT DOCUMENTATION PAGE

Form Approved
OMB No. 0704-0188

1. REPORT DATE (DD-MM-YYYY)	2. REPORT TYPE	3. DATES COVERED (From - To)
05-09-2005	REPRINT	

4. TITLE AND SUBTITLE

Evidence for an OH(υ) Excitation Mechanism of CO_2 4.3 μm Nighttime Emission from SABER/TIMED Measurements

5a. CONTRACT NUMBER

5b. GRANT NUMBER

5c. PROGRAM ELEMENT NUMBER
62601F

6. AUTHOR(S)

M. Lopez-Puertas,[1] M. Garcia-Comas,[1] B. Funke,[1] R.H. Picard,[2] J.R. Winick,[2] P.P. Winterstiner,[3] M.G. Mlynczak,[4] C.J. Mertens,[4] J.M. Russell III,[5] and L.L. Gordley[6]

5d. PROJECT NUMBER
2301

5e. TASK NUMBER
BD

5f. WORK UNIT NUMBER
A1

7. PERFORMING ORGANIZATION NAME(S) AND ADDRESS(ES)

Air Force Research Laboratory
29 Randolph Road
Hanscom AFB, MA 01731-3010

8. PERFORMING ORGANIZATION REPORT NUMBER

AFRL-VS-HA-TR-2005-1100

9. SPONSORING / MONITORING AGENCY NAME(S) AND ADDRESS(ES)

10. SPONSOR/MONITOR'S ACRONYM(S)

AFRL/VSBYB

11. SPONSOR/MONITOR'S REPORT NUMBER(S)

12. DISTRIBUTION / AVAILABILITY STATEMENT

Approved for Public Release; Distribution Unlimited.

[1]Instituto de Astrofisica de Andalucia (CSIC), Granada, Spain
[2]Air Force Research Laboratory, Hanscom AFB, MA, USA
[3]ARCON Corporation, Waltham, MA, USA
[4]NASA Langley Research Center, Hampton, VA, USA
[5]Hampton University, Hampton, VA, USA
[6]GATS Inc., Newport News, VA, USA

13. SUPPLEMENTARY NOTES

Reprinted from: Journal of Geophysical Research, Vol. 109, D09307, doi: 10.1029/2003JD004383, 2004

14. ABSTRACT

The SABER instrument on board the TIMED satellite, successfully launched on 7 December 2001, measures the CO_2 4.3 μm atmospheric emission at day and night, from the troposphere up to the thermosphere, with a near global latitude coverage and with a very high signal-to-noise ratio. SABER has also three channels near 15 μm for the measurements of the pressure-temperature structure and two channels around 2.0 and 1.6 μm, mainly sensitive to the OH(υ ≤9) overtone radiation from levels υ = 8-9 and υ = 3-5, respectively. In this paper we analyze the measurements of SABER in channel 7, centered near 4.3 μm, taken at night in the upper mesosphere and lower thermosphere under quiet (nonauroral) conditions. The measurements of the 4.3 μm radiance in this region are much larger than expected under local thermodynamic equilibrium (LTE) and show a strong correlation with the OH channel signal. It was proposed by *Kumer et al.* [1978] that the CO_2 (υ3) levels, responsible for the emission at 4.3 μm, were excited from OH(υ) via vibrational-vibrational energy transfer with N2(1) and hence to CO_2 (υ3). SABER data (measuring simultaneously pressure, temperature, CO_2 4.3 μm emission, and OH(υ) near-IR emission) offer an unprecedented data set for understanding the non-LTE excitation mechanisms of CO_2 (υ3) in the nighttime mesosphere. We have investigated the SABER 4.3 μm radiances with the help of a non-LTE radiative transfer model for CO_2 and found that the large radiances can be explained by a fast and efficient energy transfer rate from OH(υ) to N_2(l) to CO_2 (υ3), whereby, on average, 2.8-3 N_2(l) vibrational quanta are excited after quenching of one OH(υ) molecule. A series of alternative excitation mechanisms that may enhance the nighttime 4.3 μm limb radiance were considered and found to be insignificant. The mechanism(s) whereby the energy is transferred from OH(υ) to N_2(υ) is (are) still uncertain. The populations of OH(υ) are not significantly affected by incorporation of this fast transfer since N_2 quenching of OH(υ) is negligible when compared to O_2 quenching.

15. SUBJECT TERMS

Mesosphere CO_2 4.3 μm emission OH

16. SECURITY CLASSIFICATION OF:			17. LIMITATION OF ABSTRACT	18. NUMBER OF PAGES	19a. NAME OF RESPONSIBLE PERSON
a. REPORT	b. ABSTRACT	c. THIS PAGE			Richard H. Picard
UNCLAS	UNCLAS	UNCLAS	SAR	14	19b. TELEPHONE NUMBER (include area code) 781-377-2222

JOURNAL OF GEOPHYSICAL RESEARCH, VOL. 109, D09307, doi:10.1029/2003JD004383, 2004

Evidence for an OH(υ) excitation mechanism of CO_2 4.3 μm nighttime emission from SABER/TIMED measurements

M. López-Puertas,[1] M. García-Comas,[1] B. Funke,[1] R. H. Picard,[2] J. R. Winick,[2] P. P. Wintersteiner,[3] M. G. Mlynczak,[4] C. J. Mertens,[4] J. M. Russell III,[5] and L. L. Gordley[6]

Received 25 November 2003; revised 12 February 2004; accepted 17 March 2004; published 13 May 2004.

[1] The SABER instrument on board the TIMED satellite, successfully launched on 7 December 2001, measures the CO_2 4.3 μm atmospheric emission at day and night, from the troposphere up to the thermosphere, with a near global latitude coverage and with a very high signal-to-noise ratio. SABER has also three channels near 15 μm for the measurements of the pressure-temperature structure and two channels around 2.0 and 1.6 μm, mainly sensitive to the OH($\upsilon \leq 9$) overtone radiation from levels $\upsilon = 8-9$ and $\upsilon = 3-5$, respectively. In this paper we analyze the measurements of SABER in channel 7, centered near 4.3 μm, taken at night in the upper mesosphere and lower thermosphere under quiet (nonauroral) conditions. The measurements of the 4.3 μm radiance in this region are much larger than expected under local thermodynamic equilibrium (LTE) and show a strong correlation with the OH channel signal. It was proposed by *Kumer et al.* [1978] that the $CO_2(\upsilon_3)$ levels, responsible for the emission at 4.3 μm, were excited from OH(υ) via vibrational-vibrational energy transfer with $N_2(1)$ and hence to $CO_2(\upsilon_3)$. SABER data (measuring simultaneously pressure, temperature, CO_2 4.3 μm emission, and OH(υ) near-IR emission) offer an unprecedented data set for understanding the non-LTE excitation mechanisms of $CO_2(\upsilon_3)$ in the nighttime mesosphere. We have investigated the SABER 4.3 μm radiances with the help of a non-LTE radiative transfer model for CO_2 and found that the large radiances can be explained by a fast and efficient energy transfer rate from OH(υ) to $N_2(1)$ to $CO_2(\upsilon_3)$, whereby, on average, 2.8–3 $N_2(1)$ vibrational quanta are excited after quenching of one OH(υ) molecule. A series of alternative excitation mechanisms that may enhance the nighttime 4.3 μm limb radiance were considered and found to be insignificant. The mechanism(s) whereby the energy is transferred from OH(υ) to $N_2(\upsilon)$ is (are) still uncertain. The populations of OH(υ) are not significantly affected by incorporation of this fast transfer since N_2 quenching of OH(υ) is negligible when compared to O_2 quenching. *INDEX TERMS:* 0310 Atmospheric Composition and Structure: Airglow and aurora; 0317 Atmospheric Composition and Structure: Chemical kinetic and photochemical properties; 0340 Atmospheric Composition and Structure: Middle atmosphere—composition and chemistry; *KEYWORDS:* mesosphere, CO_2, 4.3 μm emission, OH

Citation: López-Puertas, M., M. García-Comas, B. Funke, R. H. Picard, J. R. Winick, P. P. Wintersteiner, M. G. Mlynczak, C. J. Mertens, J. M. Russell III, and L. L. Gordley (2004), Evidence for an OH(υ) excitation mechanism of CO_2 4.3 μm nighttime emission from SABER/TIMED measurements, *J. Geophys. Res.*, *109*, D09307, doi:10.1029/2003JD004383.

1. Introduction

[2] An accurate knowledge of the CO_2 4.3 μm radiance in the nighttime quiet mesosphere is important to allow for an accurate retrieval of the CO_2 volume mixing ratio (vmr) at night.

[3] Whereas the processes responsible for nonlocal thermodynamic equilibrium (non-LTE) emissions of CO_2 at 4.3 μm are well-known for daytime conditions [e.g., *López-Puertas and Taylor*, 2001], nighttime models have been much less successful. The principal processes contributing to the non-LTE populations in the mesosphere at

[1]Instituto de Astrofísica de Andalucía (CSIC), Granada, Spain.
[2]Air Force Research Laboratory, Space Vehicles Directorate, Hanscom AFB, Massachusetts, USA.
[3]ARCON Corporation, Waltham, Massachusetts, USA.
[4]NASA Langley Research Center, Hampton, Virginia, USA.
[5]Center for Atmospheric Sciences, Hampton University, Hampton, Virginia, USA.
[6]GATS Inc., Newport News, Virginia, USA.

0148-0227/04/2003JD004383$09.00

night are radiative transfer and rapid vibrational-vibrational (V-V) transfer between CO_2 and N_2, e.g.,

$$N_2(1) + CO_2 \overset{k_1}{\leftrightarrow} N_2 + CO_2(\upsilon_3). \quad (1)$$

It was also proposed by *Kumer et al.* [1978] that $CO_2(\upsilon_3)$ is excited from vibrationally excited $OH(\upsilon \leq 9)$ in the upper mesosphere at night through vibrational energy transfer via $N_2(1)$, that is,

$$OH(\upsilon) + N_2 \overset{k_2}{\rightarrow} OH(\upsilon - 1) + N_2(1), \quad (2)$$

followed by reaction (1).

[4] It has been reported recently that the CO_2 vmr declines at altitudes lower than previously thought [*López-Puertas et al.*, 1998b, 2000; *Kaufmann et al.*, 2002] and that the homopause, where the atmosphere ceases to be well mixed, lies considerably below the accepted altitude of ~100 km. Moreover, general circulation models predict significant depletions of CO_2 in the nighttime polar winter [*Roble*, 2000]. SABER measurements of 4.3 μm emission cover nearly the entire globe, providing information about this distribution. However, the retrieval of CO_2 vmr at night depends upon a complete understanding of all the non-LTE processes populating the emitting states, including those mentioned above.

[5] The first evidence of the excitation of $CO_2(\upsilon_3)$ from $OH(\upsilon)$ via the mechanisms (1) and (2) above was given by *Kumer et al.* [1978] from the analysis of rocketborne CO_2 4.3 μm zenith radiance measurements. In that case, neither pressure and temperature nor $OH(\upsilon \leq 9)$ emission were simultaneously measured with the CO_2 4.3 μm radiance. Later, the SPIRE experiment [*Stair et al.*, 1985] measured simultaneously CO_2 4.3 μm radiance and $OH(\upsilon)$. It was found, however, that the excitation from $OH(\upsilon \leq 9)$ with the standard quenching rates, although giving a significant contribution, was not sufficient to explain the unusually high CO_2 4.3 μm nighttime radiances [*Wintersteiner et al.*, 1990; *Kumer*, 1991]. The SPIRE measurements were taken close to the terminator. Hence one possible reason why the excitation from $OH(\upsilon)$ alone was not sufficient to explain the large radiance could be the existence of mechanisms operating at twilight (e.g., excitation of $N_2(\upsilon)$ from $O(^1D)$), or the partial illumination of the limb line-of-sight.

[6] In the CIRRIS-1A Space Shuttle experiment in 1991, there is spectral evidence of the $OH(\upsilon)$ population taken simultaneously with CO_2 4.3 μm spectra [*Wintersteiner et al.*, 1996] from the interferometer on CIRRIS-1A. In addition, there is data very similar to the SPIRE data from the 4.3 μm SPIRIT 3 radiometers, plus $OH(\upsilon)$ data from the 2.7 μm radiometer. In the 4.3 μm region CIRRIS spectra, there is sufficient spectral resolution (near 1 cm^{-1}, unapodized) to spectrally isolate the individual OH rotational lines of several Meinel bands and, hence, to specify $OH(\upsilon)$ populations. Comparison with non-LTE model calculations, using Kumer's rate for excitation of $N_2(\upsilon)$ during $OH(\upsilon)$ quenching by N_2 [*Kumer et al.*, 1978], results in underprediction of most CO_2 bands in the 4.3 μm region by about 35%.

[7] The SABER instrument on board the TIMED satellite measures the CO_2 4.3 μm atmospheric emission in daytime and nighttime, from the troposphere up to the thermosphere, and with a near global latitude coverage. In addition, SABER has three channels near 15 μm which enable the retrieval of pressure-temperature from the lower stratosphere up to about 100 km, and also two channels at around 2.0 and 1.6 μm which are mainly sensitive to the $OH(\upsilon \leq 9)$ overtone-band radiation from levels $\upsilon = 8-9$ and $\upsilon = 3-5$, respectively. Thus SABER measurements constitute an unprecedented database which allows us to substantially improve our understanding of the non-LTE excitation mechanisms of $CO_2(\upsilon_3)$ in the nighttime mesosphere.

[8] In the next section we describe the main characteristics of the SABER CO_2 4.3 μm nighttime emission under nonauroral conditions and its correlation with the emission measured in the OH channels. In section 3 we describe the model. In section 4 we discuss the analysis and interpretation of the measurements and conclude in section 5.

2. Measurements

[9] SABER is a 10-channel wideband infrared radiometer launched on board the NASA TIMED satellite on 7 December 2001. TIMED is flying in a circular orbit at 625 km altitude with an inclination of 74.1° that precesses with the ascending node passing through all local times in a period of 65 days. SABER measures the atmospheric limb radiances from the lower stratosphere up to the upper thermosphere over the latitude range from 52°S to 83°N, with alternate coverage from 83°S to 52°N every 2 months [*Russell et al.*, 1999]. This requirement for alternating coverage is the result of a yaw maneuver that must be performed regularly as the orbit precesses in order to keep the SABER instrument's aperture on the cold side of the TIMED spacecraft looking away from the Sun. SABER takes about one hundred limb scans per orbit with about 15 orbits per day. The spectral responses of channels 7, 8 and 9, measuring, respectively, the CO_2 4.3 μm, the OH 2.0 μm and the OH 1.6 μm emissions, are shown in the work of *Russell et al.* [1999]. A more detailed description of SABER performance is also included in that reference. Typical profiles of the CO_2 4.3 μm atmospheric nighttime limb radiances as measured by SABER are shown in Figure 1. The signal-to-noise (S/N) ratio for the CO_2 4.3 μm channel is greater than one up to about 130 km at nighttime under quiescent conditions, and up to about 180 km during daytime. The vertical resolution is about 2 km.

[10] As is discussed in section 3, the populations of the CO_2 vibrational levels emitting in the 4.3 μm region are in local thermodynamic equilibrium (LTE) in the stratosphere and lower mesosphere and break down from LTE in the upper mesosphere, where they are largely populated by the absorption of upwelling radiation. Hence their populations and, in consequence, the radiance they emit at upper mesospheric levels is significantly correlated to the temperature in the lower mesosphere. This effect is clearly seen in SABER data. Figure 1 shows a typical example illustrating this effect. We see that, while the 15 μm radiance profiles, responding mostly to temperature, are similar for scans 21 and 30 (or larger for scan 30) at upper mesospheric tangent heights, they differ by about 50% (~26 K when translated into temperature, with scan 21 larger) in the lower mesosphere. The 4.3 μm radiance profiles are, however, not only

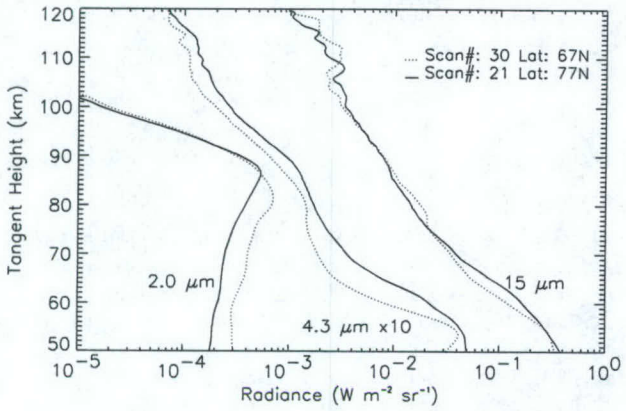

Figure 1. Two typical profiles of (left) OH 2.0 μm, (middle) CO_2 4.3 μm, and (right) CO_2 15 μm limb radiances for nighttime measured by SABER. The measurements were taken on 28 January 2002, orbit 762, at latitudes of 67°N (scan 30) (dotted) and 77°N (scan 21) (solid). The 4.3 μm radiances have been multiplied by a factor of 10.

significantly different in the lower mesosphere, but also in the upper mesosphere (with scan 21 larger), showing the correlation of upper-mesospheric 4.3 μm radiance with temperature in the lower mesosphere. As is shown below, the CO_2 4.3 μm radiance is also significantly enhanced in the upper mesosphere by the non-LTE excitation from OH(υ) via collisions with N_2. The OH radiance profile measured by SABER in scan 21 is, however, significantly smaller than in scan 30 (Figure 1), hence disproving that the larger 4.3 μm radiance in scan 21 is caused by an enhanced OH(υ) population. To illustrate that this effect is generally present, we show in Figure 2 a correlation plot of the CO_2 4.3 μm radiance (channel 7) around the mesopause (85 km) with the CO_2 15 μm radiance (channel 1) at the lower mesosphere (55–65 km). Four panels have been plotted for different values of the OH radiance emission in order to discriminate this effect from the correlation with the OH emission (see below). The correlation between these two CO_2 radiances is apparent from the figure. SABER data then show that an accurate analysis of the CO_2 4.3 μm upper mesospheric radiance requires temperature measurements not only in this region but also in the upper stratosphere and lower mesosphere.

[11] The data also show clearly the correlation between the CO_2 4.3 μm radiances in the mesosphere and lower thermosphere and those measured in the OH channels. A typical example is shown in Figure 3. Larger CO_2 4.3 μm limb radiances around the OH layer (~85 km) are correlated with the larger OH radiances measured in the OH channel at 2.0 μm. The 15 μm radiances up to 65 km (not shown) are virtually identical for the three scans. The stratopause and lower mesosphere temperatures for scans 3 and 94 are less than 3 K different from that of scan 98. This difference makes a change of less than 5% in the 4.3 μm radiance at 85 km, much less than the observed ~100% difference.

[12] A statistical analysis of the measurements including all nighttime scans for 4 orbits, covering all latitudes and equinox and solstice periods (more than 200 scans) is shown in Figure 4, which clearly manifests this correlation. This strongly suggests that the large CO_2 4.3 μm nighttime emission measured by SABER at the upper mesospheric tangent heights is produced either directly or indirectly by the vibrationally excited OH(υ). We note also that $\Delta\upsilon = 1$ radiation in the Meinel bands from the high-lying vibrational levels of OH falls into the 4.3 μm SABER bandpass. However, as we will see below, the direct OH Meinel-band

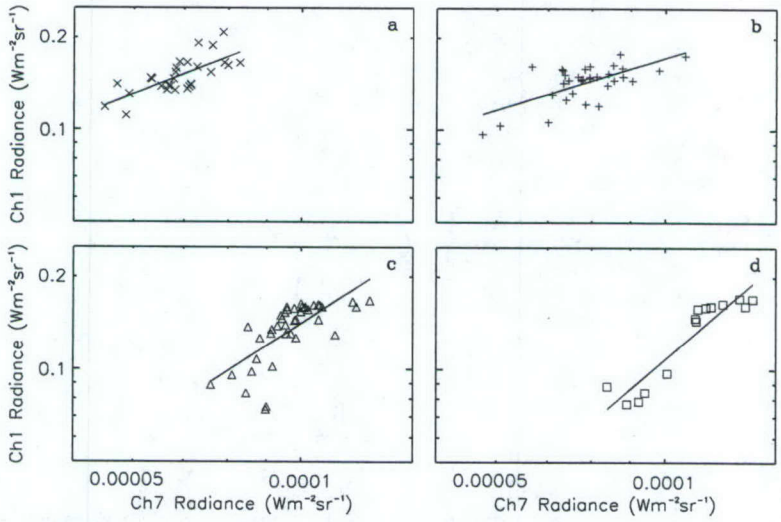

Figure 2. Correlation between the CO_2 4.3 μm radiance (channel 7) at 85 km (abscissa) and the mean radiance of CO_2 near 15 μm (channel 1) in the 55–65 km interval (ordinate). The different panels show this correlation for different values of the radiance measured in channel 8 (OH 2.0 μm emission): (a) 3–4, (b) 4–5, (c) 6–7, and (d) 7–8 in units of 10^{-4} W m^{-2} sr^{-1}. The measurements correspond to all nighttime scans measured in orbits 1264 (3 March), 3046 (1 July), 4272 (22 September), and 3098 (4 July).

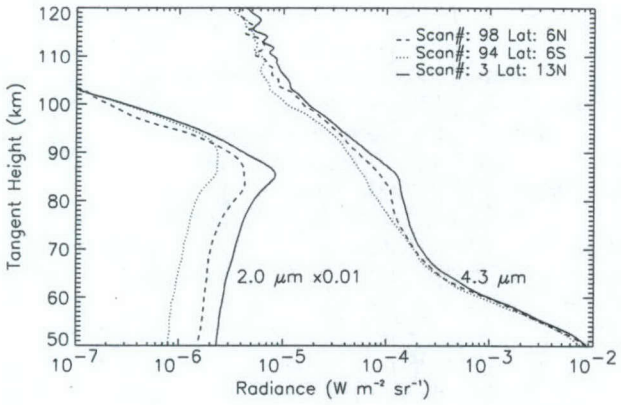

Figure 3. Correlation between the (right) CO_2 4.3 μm and (left) OH 2.0 μm nighttime limb radiances. The OH profiles have been scaled by a factor of 0.01. The measurements were taken on 1 July 2002, orbit 3048, at latitudes of 6°S (dotted), 6°N (dashed), and 13°N (solid), with solar zenith angles of 148°, 136°, and 130°.

emission is insufficient by itself to account for the correlation between the OH(υ) channels and the 4.3 μm channel.

3. Model Inputs

[13] The analysis of the measurements requires reference atmospheres (pressure, temperature, and constituent abundances), the populations of the OH(υ ≤ 9) levels, a CO_2 non-LTE model that calculates the populations of the CO_2 energy levels emitting near 4.3 μm, and a forward radiative transfer code to compute limb radiances under non-LTE conditions.

[14] The pressure-temperature profiles (p-T) have been taken from the non-LTE inversion of the SABER measurements at 15 μm in channels 1 and 3 [*Mertens et al.*, 2002]. Nighttime data from version 1.03 were used in this study which retrieves p-T but assumes the CO_2 vmr profile. Temperature is retrieved from SABER up to about 105 km with 1-σ precision smaller than 2 K in the stratosphere and lower mesosphere and about 3.5 K at 80 km. Above 105 km, SABER temperatures were merged on a pressure scale with those predicted by the TIME-GCM model [*Roble*, 2000] for the geolocations corresponding to the measurements. A typical temperature profile is shown in Figure 7, together with the vibrational temperatures of several CO_2 levels, and temperature fields are also shown below (see Figures 12 and 13).

[15] To calculate the CO_2 vibrational temperatures and radiance profiles the CO_2 volume mixing ratio (vmr) is required. The nominal CO_2 vmr used in the preliminary non-LTE temperature retrieval was also used here, i.e., the TIME-GCM model predictions. Also, a sensitivity study using a smaller CO_2 vmr as suggested by the recent satellite measurements of ISAMS and CRISTA [*López-Puertas et al.*, 1998b; *Zaragoza et al.*, 2000; *López-Puertas et al.*, 2000; *Kaufmann et al.*, 2002] has been performed and is discussed below. The atomic oxygen is also necessary for calculating the populations of both the CO_2 15 μm levels, which are required for performing the non-LTE temperature retrievals, and the 4.3 μm levels in the lower thermosphere. Its concentration will be derived from the SABER O_2 1.27 μm channel below about 100 km. In that region, however, it has little effect on the populations of the CO_2 levels emitting at 4.3 μm. Hence, in the absence of measurements at higher altitudes, the $O(^3P)$ was taken from the TIME-GCM model for the whole altitude region studied here.

3.1. OH(υ ≤ 9) Populations

[16] The OH(υ ≤ 9) populations, [OH(υ)], are required in this study: (1) to compute their direct contribution to the atmospheric emission in the CO_2 4.3 μm channel, and (2b) for calculating the excitation of $CO_2(\upsilon_3)$ levels from OH (υ ≤ 9). These OH(υ) populations have been obtained from SABER OH channels 8 and 9 measurements using an Abel inversion as detailed below.

[17] The radiance at a tangent height z_t measured in the SABER OH channels, for which we can assume optically thin conditions, is given by, e.g., *López-Puertas and Taylor* [2001]

$$L(z_t) = \int_x [\mathrm{OH}(x)]_e \, G(x) \, \mathrm{d}x, \tag{3}$$

where x is the position on the limb path, which depends on z_t, $[\mathrm{OH}]_e = \sum_{\upsilon=1,9}[\mathrm{OH}(\upsilon)]$, $G(x)$ is given by

$$G(x) = \frac{h}{4\pi} \sum_{\upsilon} \Phi(\upsilon) \sum_{J} q_r(\upsilon, J) \, A_{\upsilon,J} \cdot \int_{\nu} f(\nu - \nu_{0,\upsilon,J}) \, F(\nu) \, \nu \, \mathrm{d}\nu, \tag{4}$$

h is Planck's constant, $\Phi(\upsilon)$ is the normalized vibrational distribution of level υ, $\Phi(\upsilon) = [\mathrm{OH}(\upsilon)]/[\mathrm{OH}]$, $q_r(\upsilon, J)$ is the normalized population of rotational state J in level υ, $A_{\upsilon,J}$ and $f(\nu - \nu_{0,\upsilon,J})$ are the Einstein coefficient and the normalized line shape function, respectively, for the ro-

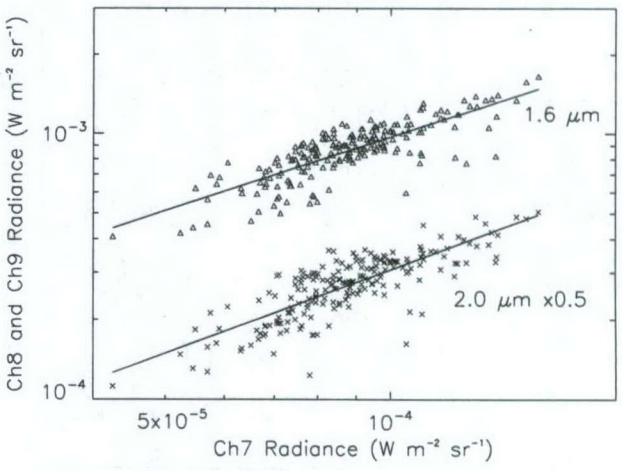

Figure 4. Correlation between the CO_2 4.3 μm radiance (abscissa) and the OH 1.6 μm (triangles) and 2.0 μm (×) limb radiances at a tangent height of 85 km for all nighttime scans measured in orbits 1264 (3 March), 3046 (1 July), 4272 (22 September), and 3098 (4 July). The OH 2.0 μm radiances (×) have been multiplied by a factor of 0.5. Solid lines are the linear fits.

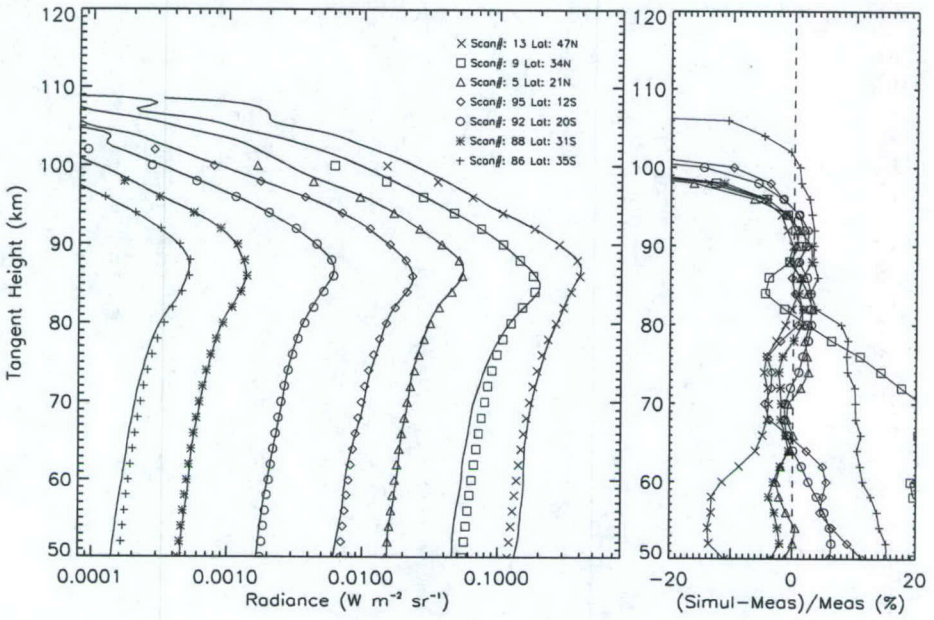

Figure 5. SABER channel 8 OH 2.0 μm radiance profiles for several latitudes at equinox conditions (orbit 1264, 3 March, 2002). (left) Measured (solid lines) and calculated with the derived OH(υ) populations (symbols). Note they are displaced from the first (left) profile by factors of 3 for a clearer representation. (right) Relative difference (computed-measured) measured in percent.

vibrational transition line at $\nu_{0,\upsilon,J}$, and $F(\nu)$ is the channel spectral response. Note that $\Phi(\upsilon)$, $q_r(\upsilon, J)$, and $f(\nu - \nu_{0,\upsilon,J})$ are all x-dependent, even though the x dependence has not been stated explicitly. From equation (3) we see that the measured radiance is proportional to $[OH]_e$, and the radiances can be inverted using the Abel method as follows. Discretizing equation (3) we get

$$L_i = \sum_j C_{ij}\,[OH]_{e,j}\,G_j, \tag{5}$$

where indexes i and j run over the tangent heights and altitudes, respectively, and the matrix C_{ij} accounts for the geometric factors of the integration along the line of sight. Writing equation (5) in vector form we get $\mathbf{L} = C\{[\mathbf{OH}]_e\mathbf{G}\}$, and by inverting this is found:

$$[\mathbf{OH}]_e\mathbf{G} = C^{-1}\mathbf{L}. \tag{6}$$

[18] Using this equation, the $[OH(z, \upsilon)]$ vertical density profiles derived from a radiance profile measured in the SABER OH channels, $\mathbf{L}$, are computed by

$$[OH(z,\upsilon)]_j = [OH_{ref}(z,\upsilon)]_j \frac{\left(C^{-1}\mathbf{L}\right)_j}{\left(C^{-1}\mathbf{L}_{ref}\right)_j}, \tag{7}$$

where $[OH_{ref}(z, \upsilon)]$ is a reference set of OH(υ) density profiles, and $\mathbf{L}_{ref}$ is the radiance computed with $[OH_{ref}(\upsilon, z)]$ and the measured pressure-temperature profile. Hence we have assumed that $\mathbf{G}$ changes very little between the reference and actual situations. There are nine OH($\upsilon = 1-9$) number density profiles (unknowns) but we only have 2 channels, the 2.0 μm and 1.6 μm, which are sensitive to the populations of OH $\upsilon = 8-9$ and $\upsilon = 3-5$ levels, respectively. The process above was repeated for each of the two SABER OH channels. The number densities for the OH($\upsilon = 6-9$) levels were obtained using the measurements in the 2.0 μm channel, and those of levels $\upsilon = 1-5$ from that in the 1.6 μm channel. The $[OH_{ref}(z, \upsilon)]$ reference profiles were calculated with a photochemical model very similar to those developed by *Makhlouf et al.* [1995] and *Adler-Golden* [1997], including the rate constants for the production and quenching processes from Adler-Golden, and assuming the single quantum quenching of OH(υ) by O_2. A test case on the effects of assuming a rather different vibrational distribution for the $[OH_{ref}(z, \upsilon)]$ reference profiles, that is, those calculated assuming the multi-quantum quenching of OH(υ) by O_2, was carried out and found to have very small effects ($\leq 2-3\%$) on the simulated 4.3 μm radiances. A few tests were also carried out to verify that the derived OH(υ) populations fit the measured OH radiances in both channels. Figures 5 and 6 show some examples. These clearly manifest that the derived OH(υ) populations reproduce the measurements very well, within 5% at the altitudes of the OH layer.

3.2. $CO_2(\upsilon_3)$ Populations

[19] The populations of the $CO_2(\upsilon_3)$ vibrational levels have been computed using the non-LTE model developed by *López-Puertas et al.* [1998a, 1998b] with the updates described in the work of *López-Puertas and Taylor* [2001] and P. P. Wintersteiner et al. (manuscript in preparation, 2004). We have intercompared this model extensively with other codes (P. P. Wintersteiner et al., manuscript in preparation, 2004) and found very small differences (below 1 K) in the vibrational temperatures. The rate constants reported in the above references have been used here except for the

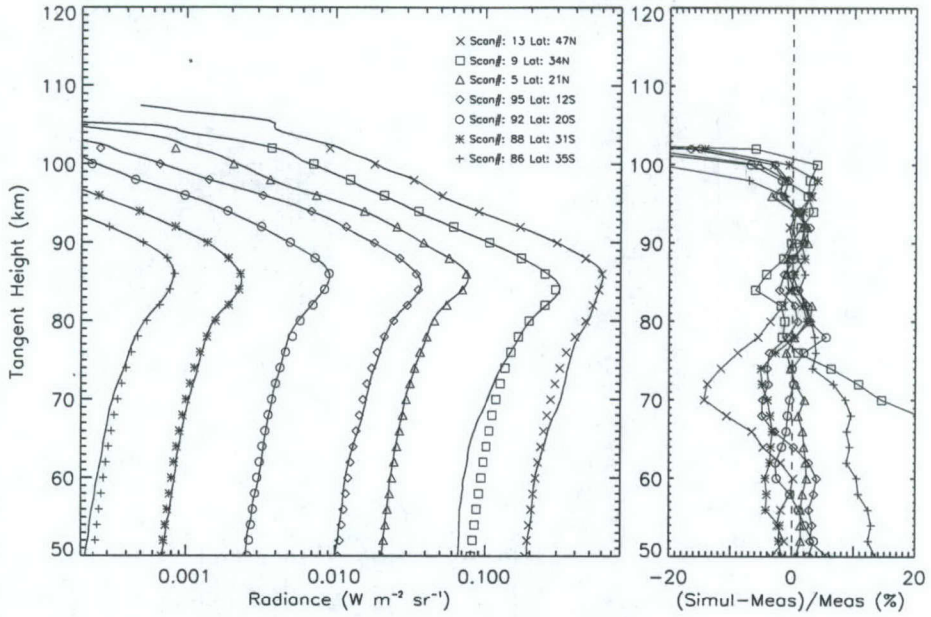

Figure 6. As in Figure 5 but for the SABER channel 9 OH 1.6 μm radiance profiles.

vibrational relaxation of OH($\upsilon \leq 9$) by N_2 (process (2)) which was taken, consistent with the OH photochemical model, from *Adler-Golden* [1997]. A typical result of the model for the vibrational temperatures of the $CO_2(\upsilon_3)$ levels that mainly contribute to channel 7 radiance is shown in Figure 7. We also show in that figure the effects of the OH(υ) excitation mechanism (processes (2) and (1)). The excitation has a large impact on the $CO_2(\upsilon_3)$ level populations in the upper mesosphere. The most enhanced population is that of the (00^01) level of the main isotope with an

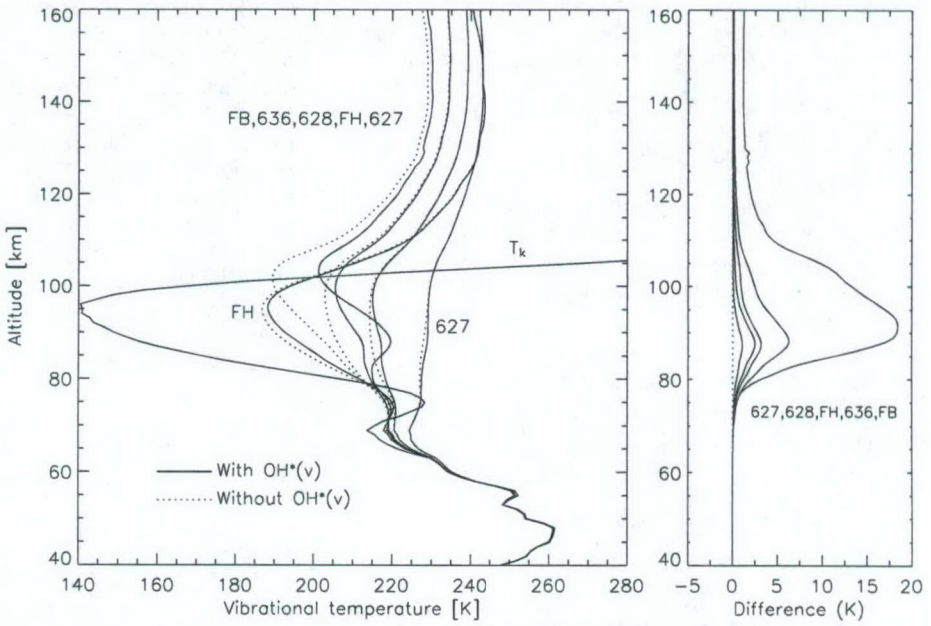

Figure 7. Vibrational temperatures (T_υs) of the $CO_2(\upsilon_3)$ levels that mainly contribute to the SABER channel 7 radiance near 4.3 μm for the kinetic temperature profile (T_k) measured by SABER on 1 July 2002 at a latitude of 30°N (orbit 3046, scan 6). Dotted lines are the T_υs without OH(υ) excitation and solid lines with the OH(υ) excitation with the rates for process (2) taken from *Adler-Golden* [1997]. The right panel shows the differences in the vibrational temperatures induced by the OH excitation. The plots labeled by isotope numbers (636, 628, 627) refer to their (00^01) levels; fundamental band (FB) and first hot (FH) refer, respectively, to the (00^01) and (01^11) levels of the main 626 isotope.

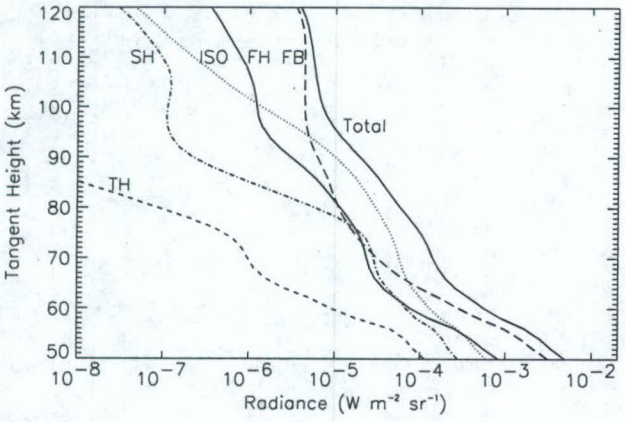

Figure 8. Contributions of the major CO_2 4.3 μm bands to the SABER channel 7 radiances for the case study of Figure 7. The OH(υ) excitation was included with the rate constants of *Adler-Golden* [1997]. FB (dash), FH (dash-dot-dot-dot), SH (dash-dot), and TH (short-dash) are the contributions of fundamental, first hot, second hot, and third hot bands of the major 626 isotope, respectively. ISO (dotted) is the contribution of all the isotopic bands included in the calculations (see Table 1).

increase in its vibrational temperature of about 20 K around 90 km. It is noticeable that the population of this level is enhanced not only at the altitude of the local excitation of CO_2 from OH(υ), a layer about 10 km thick around 85 km, but also at higher altitudes, due to radiative transfer in the ν_3 bands of CO_2. Similar behavior at 4.3 μm is also noted above other sources of excitation producing discrete Chapman-like layers of enhanced radiating states. These include excitation by auroral electrons [*Winick et al.*, 1987; *Picard et al.*, 1987; *Winick et al.*, 1988] or electrons energized by thundercloud electric fields [*Picard et al.*, 1997]. This radiative transport of the excitation to higher altitudes above a layered source, as will be discussed later, is important for understanding the radiance measured by SABER at altitudes above the OH mesospheric layer. The enhancements in the other $CO_2(\upsilon_3)$ contributing levels are much smaller, varying between peak values of 7 and 1 K for the second to the fourth minor isotopes. The excitation in the major isotope (01^11) level is also significant, about 3 K at the OH layer peak. It is also important to note that the effect of the local temperature in this region on the radiance is small. Thus the populations of the levels do not follow closely the peak in the kinetic temperature inversion layer around 75 km.

4. Analysis of the Measurements

[20] With all necessary inputs, the radiances in the SABER CO_2 4.3 μm channel were simulated using the KOPRA line-by-line forward radiance model [*Stiller*, 2000] and compared with measurements. We first discuss the radiances focusing on a typical profile. We show the contributions of the different CO_2 bands to this channel and then explore several excitation mechanisms capable of explaining the observations. Later we extend the study by including observations taken over several orbits covering near pole-to-pole latitudes and different seasons, including equinox and solstice conditions.

[21] Figures 8 and 9 show the contributions of the different CO_2 bands near 4.3 μm to the SABER 4.3 μm channel (see Table 1). The major contributor to the total radiance is the strongest 4.3 μm fundamental band of the major isotope (FB). In the region between about 65 and 90 km, however, the contribution of the three minor isotopes 636, 628 and 627 (ISO) together is dominant, encompassing 40–50% of the total emission. These calculations include the excitation from OH(υ) with the nominal rate for process (2). However, if this is not included, the relative contribution of these isotopic bands is even larger (up to 60%) and covers a wider altitude interval. These percentages also depend on the kinetic temperature thermal structure, with colder mesopause and warmer lower mesospheric temperature responsible for larger percentages. This region of largest contribution from the isotopic bands coincides with that where the excitation from OH(υ) is most important (see Figure 7). Hence the inclusion of the isotopic contributions as well as their accurate modeling is crucial for drawing conclusions about the role and magnitude of the OH(υ) excitation of the $CO_2(\upsilon_3)$ levels.

[22] The contribution from the first hot band of the major isotope (FH) is also significant, contributing about ~20% of the total radiance from around 50 km to about 100 km. The contribution of the second hot bands (SH) is also significant at these tangent heights, although smaller than the previous bands. They contribute with a fraction between 5 and 20% in this region. The radiance in the third hot (TH) bands of the 626 isotope (see Table 1) is significant only below about 65 km and always with a fraction smaller than 3%. Other CO_2 4.3 μm bands have been found to make a negligible contribution.

4.1. Comparison of Measured and Calculated Radiances: A Sample Case

[23] Figure 10 shows a typical SABER radiance CO_2 4.3 μm nighttime profile together with several simulations. The first curve (dotted) shows the radiance computed with the non-LTE retrieved pressure-temperature profile derived from SABER and the CO_2 non-LTE populations described above without the OH($\upsilon \leq 9$) excitation (process (2)). We

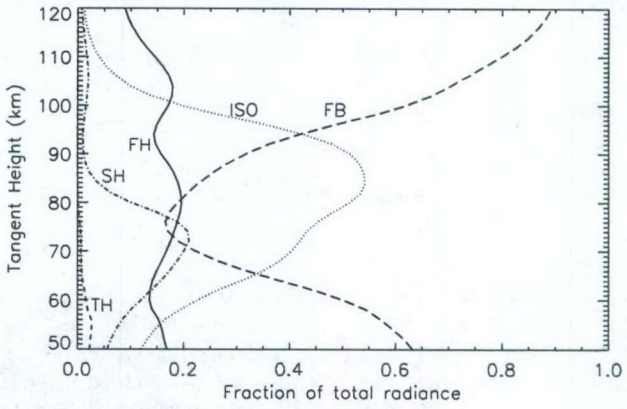

Figure 9. As in Figure 8 but with contributions of the major CO_2 4.3 μm bands to the SABER channel 7 expressed in relative percentage to the total radiance.

Table 1. Main CO_2 Bands Contributing to the 4.3 μm SABER Channel at Nighttime

Group	Isotope[a]	Upper Level[b]	Lower Level[b]	Upper Level[a]	Lower Level[a]	$\tilde{\nu}_0$, cm^{-1}	Band Strength[c]
FB	626	00^01	00^00	00011	00001	2349.143	955357.125
FH	626	01^11	01^10	01111	01101	2336.632	73666.258
SH1	626	02^21	02^20	02211	02201	2324.141	2838.857
SH2	626	02^01	02^00	10012	10002	2327.433	1789.326
SH3	626	10^01	10^00	10011	10001	2326.598	1079.329
TH1	626	03^11	03^10	11112	11102	2315.235	14.610
TH2	626	03^31	03^30	03311	03301	2311.667	10.260
TH3	626	11^11	11^10	11111	11101	2313.773	72.010
FB	636	00^01	00^00	00011	00001	2283.488	9598.150
FH	636	01^11	01^10	01111	01101	2271.760	817.848
SH1	636	02^21	02^20	02211	02201	2260.049	33.330
SH2	636	02^01	02^00	10012	10002	2261.910	19.460
SH3	636	10^01	10^00	10011	10001	2262.848	11.620
FB	628	00^01	00^00	00011	00001	2332.113	3518.852
FH	628	01^11	01^10	01111	01101	2319.738	257.879
FB	627	00^01	00^00	00011	00001	2340.014	647.575
FH	627	01^11	01^10	01111	01101	2327.581	49.683

[a]HITRAN notation.
[b]Herzberg notation.
[c]Values shown are $\times 10^{22}$ (cm^{-1}/cm^{-2}) at $T = 296$ K.

see that measured radiances are largely underpredicted. The next curve (dot-dot-dot-dash) shows the addition of the radiance emitted by OH($\upsilon \leq 9$) in the 4.3 μm channel bandpass, mainly emission from the $9 \rightarrow 8$ and $8 \rightarrow 7$ transitions. The emission of OH in the $\Delta\upsilon = 1$ was suggested by *Mlynczak and Solomon* [1993] and has been measured by the ISAMS experiment [*Zaragoza et al.*, 1998]. This direct OH(υ) contribution to the SABER radiance is very small. If we include the excitation of $CO_2(\upsilon_3)$ from OH($\upsilon \leq 9$) (processes (1) and (2)) (curve short-dash), the predicted radiance is much closer to that measured, both below the OH(υ) peak layer, because of the geometry effect in the limb radiances, and above, up to ~120 km, because of the radiative transfer in the CO_2 4.3 μm bands (see Figure 7). However, we still underpredict the measurements by about 45%, above about 80 km. We

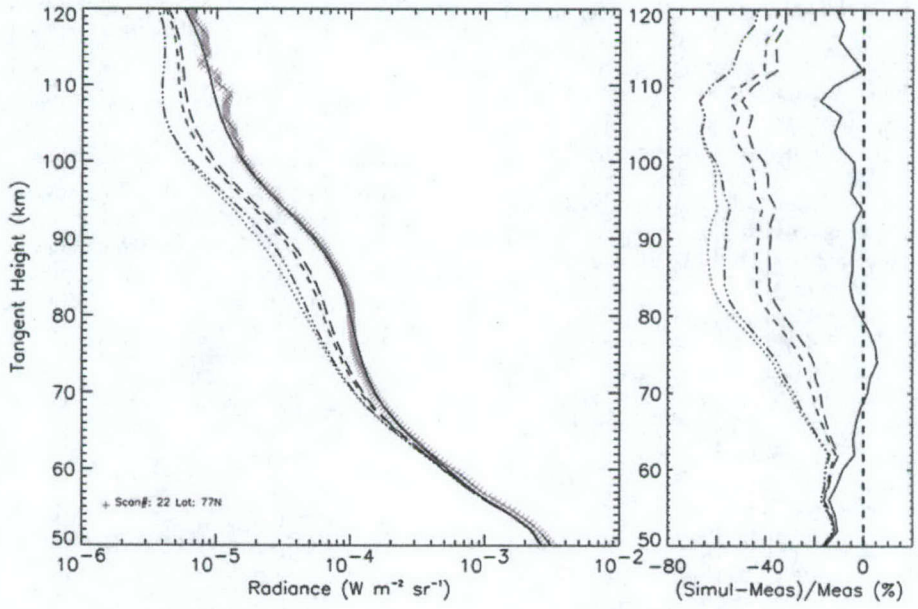

Figure 10. Measured and simulated SABER nighttime radiances in the CO_2 4.3 μm channel for the case study of 3 March 2002, scan 22 (orbit 1264) at a latitude of 77°N. (left) Measured (×) and computed radiances (lines) and (right) radiance relative difference (computed-measured)/measured in percent. Dots, CO_2 contribution without the OH(υ) excitation mechanism; dot-dot-dot-dash, the previous radiance plus the OH($\upsilon \leq 9$) direct emission in the SABER 4.3 μm channel; short dash, as previous but including excitation of CO_2 by OH(υ) via $N_2(1)$; long dash: as previous but multiplying the quenching rates of process (2) by the low temperature factor of 1.4; solid, assuming, in addition, that an average 2.8 $N_2(1)$ molecules are produced per OH(υ) molecule.

note that the SABER out-of-band spectral characteristics were specifically calibrated throughout the infrared, and used to explicitly model out-of-band contributions. These contributions were determined to be negligible (<1.0%) for all SABER channels.

[24] The previous simulation included the quenching rates of OH($\upsilon \leq 9$) by N_2, e.g., of *Adler-Golden* [1997, equation (2)], which are widely accepted. However, these rates have been measured at room temperature and it is possible that their values at the low upper-mesospheric temperatures can be larger by about a factor of 1.4 [*Adler-Golden*, 1997; *Lacoursiere et al.*, 2003]. By assuming this increase in the quenching rates (curve long-dash) we find a small increase in the radiances, but they are still too small by about 40% at ~80–100 km.

[25] Previous measurements of nighttime limb radiance in the 4.3 μm region taken by the SPIRE experiment [*Kumer*, 1991] also showed a significant underprediction in the upper mesosphere even including the OH(υ) excitation mechanism. Since those measurements were taken near the terminator, it is possible that the large measured radiances are due to partial illumination of the line of sight or to $O(^1D)$ excitation in the SPIRE near-twilight conditions. SABER measurements shown here, however, were taken on the nightside. In addition, the shape of the SABER channel 7 (CO_2 4.3 μm) radiance strongly resembles that of the OH layer (as did the enhanced SPIRE and CIRRIS-1A 4.3 μm radiance), and its strong correlation with channels 8 and 9 (OH) measurements suggest that the source of the large SABER channel 7 radiance is OH(υ). Thus we have explored several $CO_2(\upsilon_3)$ excitation mechanisms to find out if they are capable for explaining the remaining underestimation. These are discussed below.

4.2. Direct Excitation of $CO_2(\upsilon_3)$ From OH(υ)

[26] In addition to processes (1) and (2), we have also considered the direct excitation of $CO_2(\upsilon_3)$ from OH(υ), i.e.,

$$OH(\upsilon) + CO_2 \rightarrow OH(\upsilon - 1) + CO_2(\upsilon_3). \quad (8)$$

As there exists a strong vibrational coupling between $CO_2(001)$ and $N_2(1)$ (process (1)), processes (2) and (8) both enhance the $CO_2(\upsilon_3)$–$N_2(1)$ reservoir and their contributions reinforce each other in exciting the reservoir. Thus, including the rate constants for process (8), k_8 = (1.8, 4.8, 14.0, 28, 50, 100, 200, 400, 570) × 10^{-13} cm^3 s^{-1}, for υ = 1–9, respectively [*Dodd et al.*, 1991; *Chalamala and Copeland*,1993], we have found that the production of $CO_2(\upsilon_3)$ from process (8) is about 2000 times smaller than through process (2). Hence we conclude that the contribution of the former is negligible in comparison with that of process (2).

4.3. Excitation of $CO_2(\upsilon_3)$ via $O_2(1)$

[27] The $CO_2(\upsilon_3)$ levels can also be excited through the near resonant process

$$O_2(1) + CO_2(010) \rightarrow O_2 + CO_2(001), \quad (9)$$

which can take place at a rate of ~3–8 × 10^{-15} cm^3 s^{-1} [*Alexander et al.*, 1968; *Houghton*, 1969]. For this mechanism to be effective in populating the $CO_2(\upsilon_3)$ levels at nighttime, we need a large non-LTE population of $O_2(1)$. We have considered that $O_2(1)$ can be excited from OH(υ) by the process

$$O_2 + OH(\upsilon) \rightarrow O_2(1) + OH(\upsilon - 1), \quad (10)$$

with the rate constants of *Adler-Golden* [1997]. By including these processes the vibrational temperature of the $CO_2(001)$ level resulted in a maximum increase of only 2 K around 75 km. Hence this mechanism is clearly insufficient to explain the SABER 4.3 μm measurements.

4.4. Excitation of $CO_2(\upsilon_3)$ via $O_2(2)$

[28] Another mechanism considered in this study is the excitation of the upper state of the CO_2 first hot band (01^11) by $O_2(2)$, i.e.,

$$O_2(2) + CO_2 \rightarrow O_2 + CO_2(01^11). \quad (11)$$

To make this process efficient in exciting the $CO_2(\upsilon_3)$ levels, we would need a fast transfer of vibrational energy from OH(υ) to $O_2(2)$:

$$O_2 + OH(\upsilon) \rightarrow O_2(2) + OH(\upsilon'). \quad (12)$$

[29] Assuming that $O_2(2)$ is excited by process (12) with the same rate as $O_2(1)$ in process (10), and a rate of 10^{-14} cm^3 s^{-1} for process (11), we have estimated that the production of $CO_2(01^11)$ through this mechanism is slightly larger than that of $CO_2(001)$ from $O_2(1)$ (process (9)), i.e., a maximum increase of about 3 K in the population of $CO_2(01^11)$ at around 75 km. In this estimation we have not considered that $O_2(2)$ would be relaxed quickly in V-V collisions with O_2 and H_2O to produce $O_2(1)$ and $H_2O(010)$, and by thermal quenching with atomic oxygen. If these were considered, the excitation would be even smaller. We should also note that the enhancement would occur around 75 km, not at ~85 km, as is observed in SABER.

[30] It has also been suggested that $O_2(2)$ could be produced in the atomic oxygen recombination. However, given the nighttime conditions we are considering, that excitation of $O_2(2)$, if true, would occur at altitudes significantly higher than 85 km and, again, would also be quenched quickly due to the large $O(^3P)$ abundance. In summary, it seems rather unlikely that the required excitation of the $CO_2(\upsilon_3)$ levels occurs through excitation of $O_2(2)$.

4.5. An Efficient OH($\upsilon \leq 9$) → $N_2(1)$ → $CO_2(\upsilon_3)$ Excitation Mechanism

[31] Since no other alternative mechanism was found to explain the large measured radiance, and there is a strong correlation between the CO_2 4.3 μm and the OH 2.0 and 1.6 μm radiation (Figures 3 and 4), we then estimated the energy transfer rate from OH(υ) to N_2 to CO_2 required to account for the measured 4.3 μm radiances. We have found that using the current OH(υ) quenching rates [i.e., *Adler-Golden*, 1997] but increased by a low-temperature factor of 1.4, about 2.8–3 $N_2(1)$ molecules excited from each OH(υ)–N_2 collision are required to explain SABER radiances (solid curve in Figure 10). This means that the needed vibrational energy transfer from OH(υ) to $N_2(\upsilon)$ is about 3 times more efficient than in the single-quantum excitation,

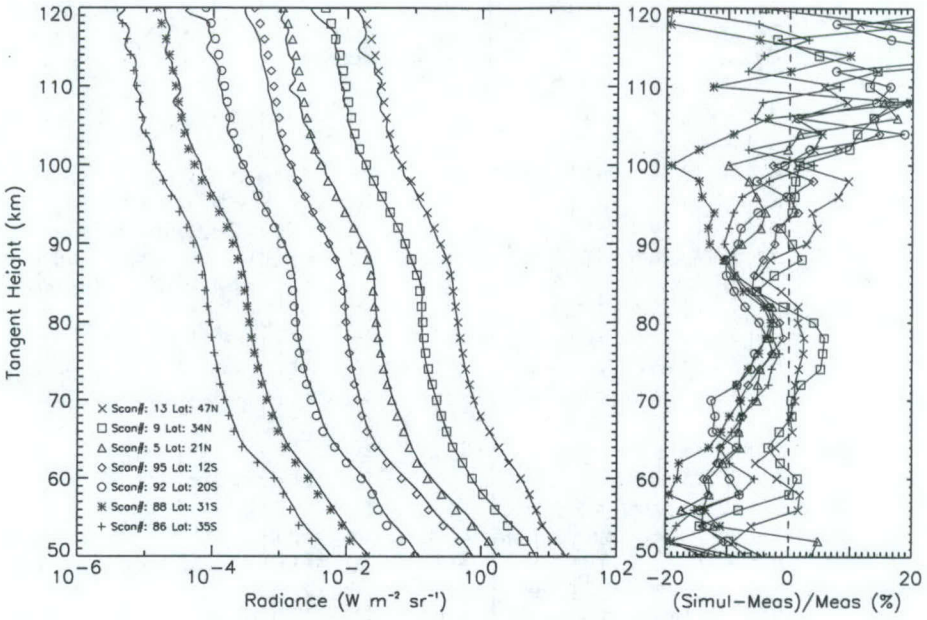

Figure 11. Measured (solid lines) and computed (symbols) SABER radiances profiles in channel 7 (CO_2 4.3 μm) for several latitudes at equinox conditions (orbit 1264, 3 March 2002). (left) Measured and computed radiances (note they are displaced from the first (left) profile by factors of 4 for a clearer representation) and (right) the relative difference (computed-measured)/measured in percent.

whereby only one $N_2(1)$ molecule is excited in every collision from each $OH(\upsilon)$ molecule (process (2)). From the point of view of the energy transfer efficiency, always considering the quenching rates of Adler-Golden (multiplied by a factor of 1.4) and typical $OH(\upsilon)$ population profiles, if, in every $OH(\upsilon)$-N_2 collision, all the vibrational energy in the $OH(\upsilon)$ system would be transferred to $N_2(1)$, an average of 8.8 $N_2(1)$ molecules would be produced. Since SABER requires 2.8–3 $N_2(1)$ molecules, a 30% efficiency in the $OH(\upsilon) \rightarrow N_2(\upsilon)$ energy transfer is required for explaining SABER radiances. This, in principle, is possible, although the mechanism(s) whereby the energy is transferred is (are) not currently known.

4.6. Comparison of Measured/Calculated Radiances: Equinox and Solstice Conditions

[32] Figure 11 shows a comparison of simulated and measured radiances for several scans of orbit 1264 taken during equinox conditions, which can be considered as typical profiles. The radiances were calculated with the energy efficiency transfer from $OH(\upsilon)$ to N_2 of 2.8 and the quenching rates of *Adler-Golden* [1997] scaled with the low temperature factor of 1.4. We see that the radiances are explained within ±15%. In the region between 70 and 90 km, where the $OH(\upsilon \leq 9)$ excitation is stronger, we get a very good agreement, within (−10, +5)%, values which are close to the systematic error estimated to be less than 5%.

[33] Below this region the radiances are underestimated by about 15%. This can be explained by the cold bias of 3–5 K found in this version (v1.03) of SABER temperatures above about 35 km, found in the comparison with Met Office assimilated analyses [*Remsberg et al.*, 2003] and several lidar data sets [*García-Comas et al.*, 2003].

[34] Above about 110 km the measured radiances are overestimated for these scans. At these altitudes, the fundamental ν_3 band is the largest contributor (see Figure 8), and becomes optically thin; hence radiance is nearly directly proportional to the CO_2 number density. Thus this small overprediction above 100 km could be well due to a difference between the real atmosphere and the TIME-GCM simulated atmosphere.

[35] In order to exclude the CO_2 vmr profile as a potential cause of the large upper mesospheric (70–100 km) radiances, we also made a CO_2 vmr sensitivity test in this region. Recent satellite measurements [*López-Puertas et al.*, 1998b; *Zaragoza et al.*, 2000; *López-Puertas et al.*, 2000; *Kaufmann et al.*, 2002] have shown that the CO_2 vmr is significantly lower than model predictions in this region. We calculated the radiances by including a lower CO_2 vmr and found that it has a small effect on the radiances. A change of ~30% in the CO_2 vmr at 90 km induces a change of only ~5% in the radiance at nearby tangent heights, essentially because the major contributor band is very optically thick at these heights. We also note that it has an opposite effect at higher tangent heights, although small too, which is induced through the $CO_2(00^01)$ population. For a smaller CO_2 vmr in the upper mesosphere, this region is more transparent to ν_3 photons, and the population of $CO_2(00^01)$ at higher altitudes, largely populated by absorption of photons emitted below in the upper mesosphere, becomes larger. Hence differences between the TIME-GCM CO_2 vmr profiles and the lower ones taken by recent satellites in the upper mesosphere induces small changes (below 5%) in this region and above.

[36] We also checked other potential sources of errors which might explain the large upper mesospheric SABER radiances, in particular non-LTE model parameters, of which the most important for nighttime conditions is the vibrational exchange rate between $N_2(1)$ and $CO_2(\upsilon_3)$, process (1). From the analysis of CO_2 4.3 μm radiance in

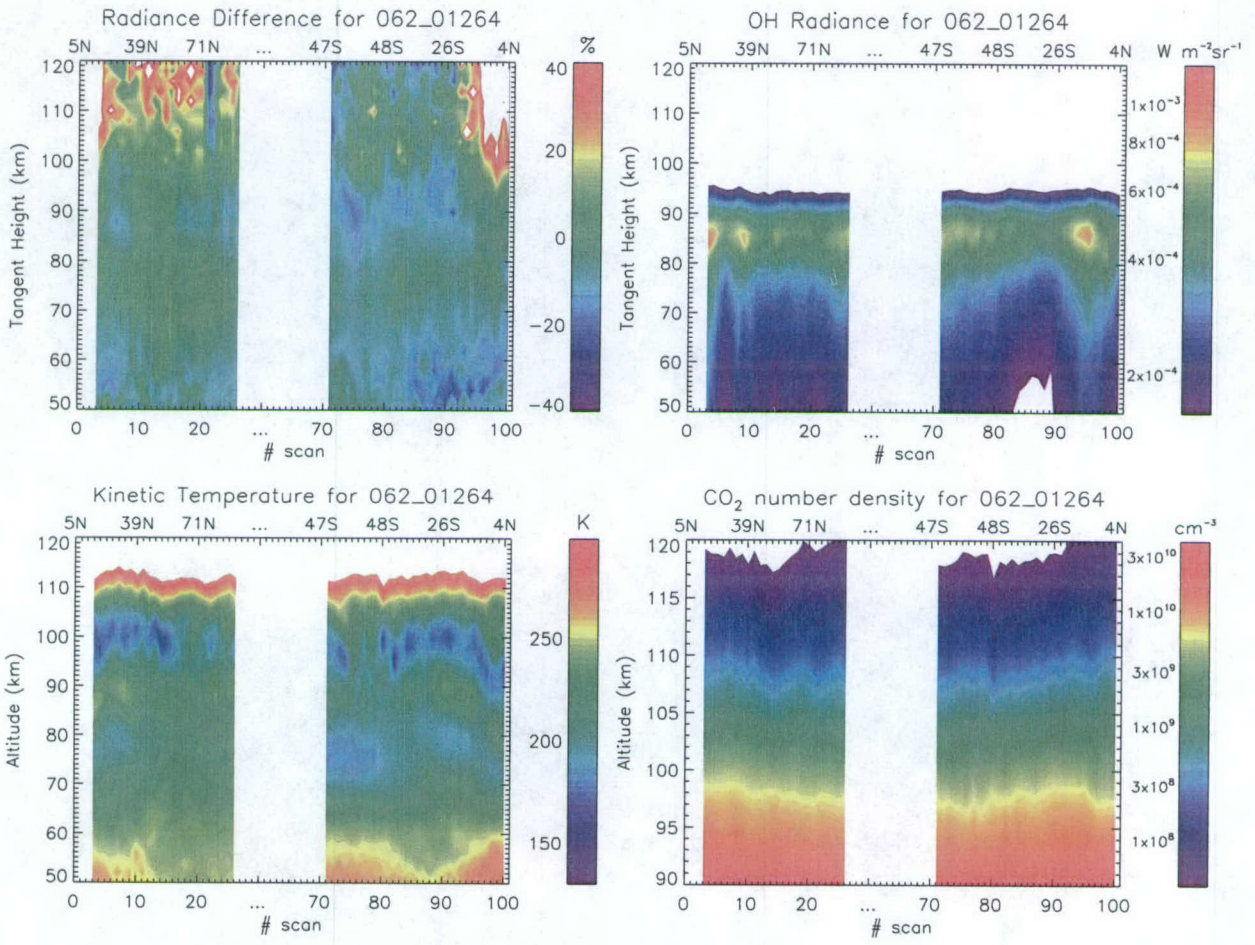

Figure 12. Panels showing the (top left) residual CO_2 4.3 μm radiance (computed-measured)/measured; (top right) the OH(υ) radiances measured in channel 8; (bottom left) the non-LTE retrieved kinetic temperature (v1.03); (bottom right) and the CO_2 number density used in the radiance calculations and temperature retrieval, for the nighttime scans of orbit 1264 taken on 3 March 2002. The white bands represent the daytime scans, not shown here. The bottom x axis shows the scan number along the orbit and the top x axis its approximate latitude.

the daytime from several instruments [i.e., *Nebel et al.*, 1994; *López-Puertas et al.*, 1998b], it has been shown that this rate is correct within narrow limits. Nevertheless we perturbed it upward by 50% and found a change in the CO_2 nighttime vibrational temperatures that was very small and of different sign for different vibrational levels. Thus, with a larger V-V transfer rate, while the vibrational temperatures of the minor isotopes and of the (01^11) levels increased about 2 K around 85 km, that of the major isotope decreased by about 1 K. We have enhancement of the minor bands at the expense of the $626(00^01)$–$N_2(1)$ system. The overall effect on the radiances is a slight increase (maximum of 3% at 85 km) when increasing the transfer rate by 50%.

[37] For completeness and generality, the study was extended to several orbits during equinox and solstice conditions. We show in Figures 12 and 13 two typical orbits for equinox and solstice conditions, respectively. Together with the residual radiances (simulated-measured), as a percentage of measured radiance, for all nighttime scans in those orbits we also show three parameters which might be correlated with the residual radiance: the OH($\upsilon \leq 9$) radiances measured by SABER (channel 8), the retrieved kinetic temperature, and the CO_2 number density used in the simulations (TIME-GCM). The residual radiances for the two orbits show the general features discussed already for Figures 10 and 11. Below 100 km the differences are confined to (+5, −15)%, with the best agreement in the region of 70–90 km. The underestimation in the lower mesosphere is smaller in equinox conditions and slightly larger in solstice conditions. By inspection of Figure 12 (top and bottom left panels) it might seem that this underestimation is correlated with higher temperatures. However, there is no evidence for a similar effect in the corresponding panels in Figure 13.

[38] In both orbits we see that the overprediction above 100 km is larger for a few of the scans (reddish and white regions). In most cases this overprediction is very closely correlated to the CO_2 number density used (lower-right panels), and so it seems that we are using a reference atmosphere (TIME-GCM) that is more dense than the actual

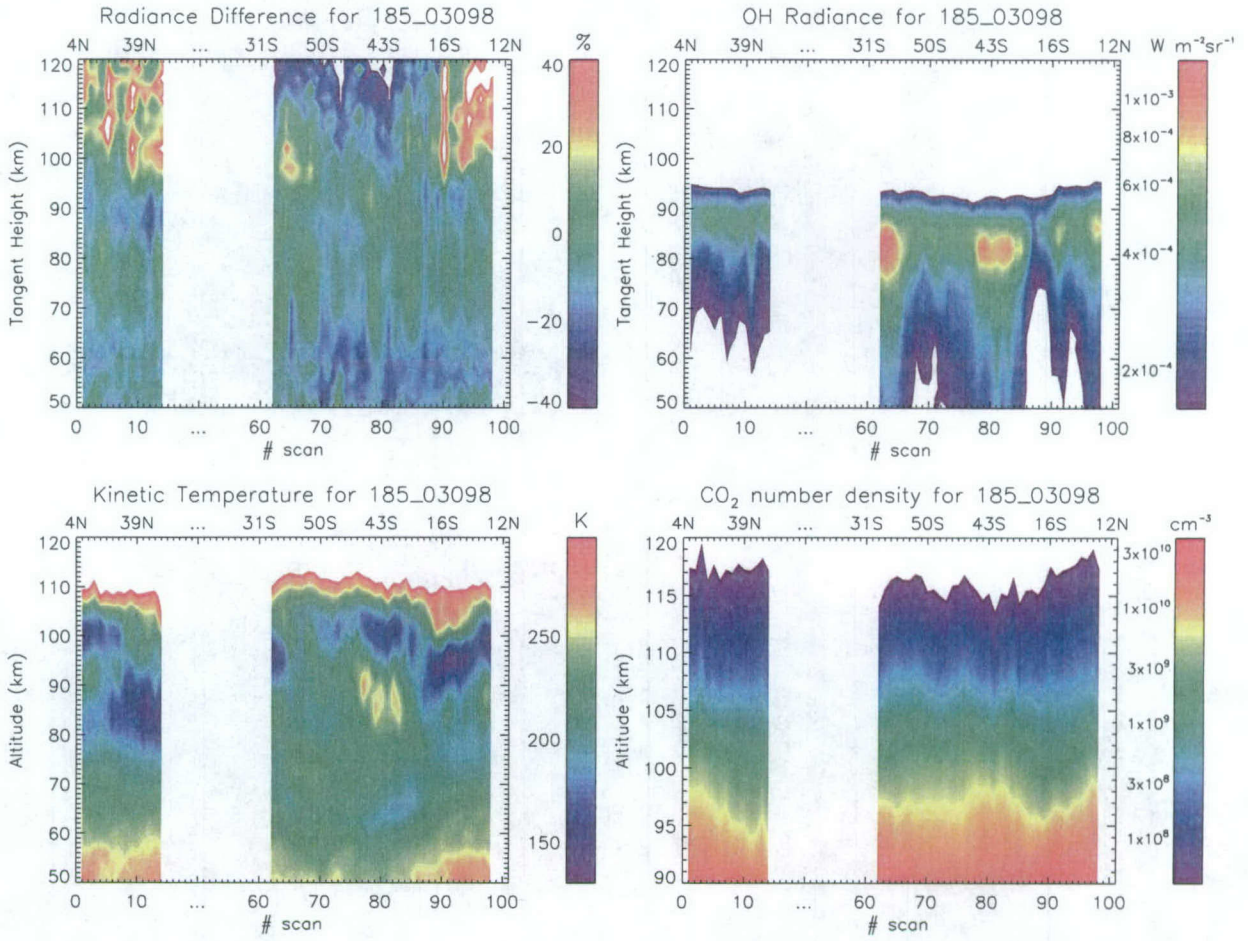

Figure 13. As in Figure 12 but for the nighttime scans of orbit 3098 taken on 4 July 2002.

atmosphere. The exception to this correlation, scans 10–20 of orbit 1264 (Figure 12), is not explained by a larger CO_2 density but, by the larger kinetic temperatures we are using (see left/bottom panel of Figure 12). The warmer temperatures produce larger vibrational temperatures, and hence larger radiances.

[39] A comparison of the residual radiances with the OH(υ) radiances in channel 8 (top-right) shows that these radiances are weakly correlated. This demonstrates that the large enhancement in the CO_2 4.3 μm measurements around 85 km and its strong correlation with the radiance in the OH channels (8 and 9) (Figures 3 and 4) is very well modeled with the proposed OH(υ)-N_2(υ) energy transfer rate.

[40] As a summary, we show in Figure 14 the mean and the standard deviation of the residual radiances for all nighttime scans of two typical orbits in equinox (March and September 2002) and another two in solstice (1 and 4 July 2002). The best agreement is found in the region where the excitation of OH(υ) is stronger, between 70 and 90 km. Even with the energy transfer efficiency of 2.8 N_2(1) molecules per OH(υ) molecule, the measured radiances are still underestimated by about 5%, which suggests that it could be slightly larger. Below 70 km the underprediction is within 5–15%, which we believe is due to a cold bias in SABER v1.03 temperatures. Note the slightly larger standard deviation in solstice conditions, as we would expect from the larger latitudinal variability. Above 95 km we slightly (5–10%) overpredict the measurements which we attribute to differences between the real atmosphere and the simulated atmosphere (TIME-GCM) we used above 100 km.

5. Conclusions

[41] From this analysis we have reached the following conclusions:

[42] 1. SABER simultaneous measurements of pressure, temperature, OH($\upsilon \leq 9$) near infrared emissions, and CO_2 4.3 μm limb radiance offer a unique and unprecedented opportunity to better understand the nighttime mesosphere and lower thermosphere.

[43] 2. The strong correlation between SABER CO_2 4.3 μm and OH 2.0 and 1.6 μm emission profiles, both in magnitude and shape of the profiles, strongly suggests that OH(υ) is the ultimate source of the larger-than-expected CO_2 4.3 μm emission.

[44] The analysis of SABER CO_2 4.3 μm nighttime mesospheric radiances under quiet (nonauroral) conditions shows that:

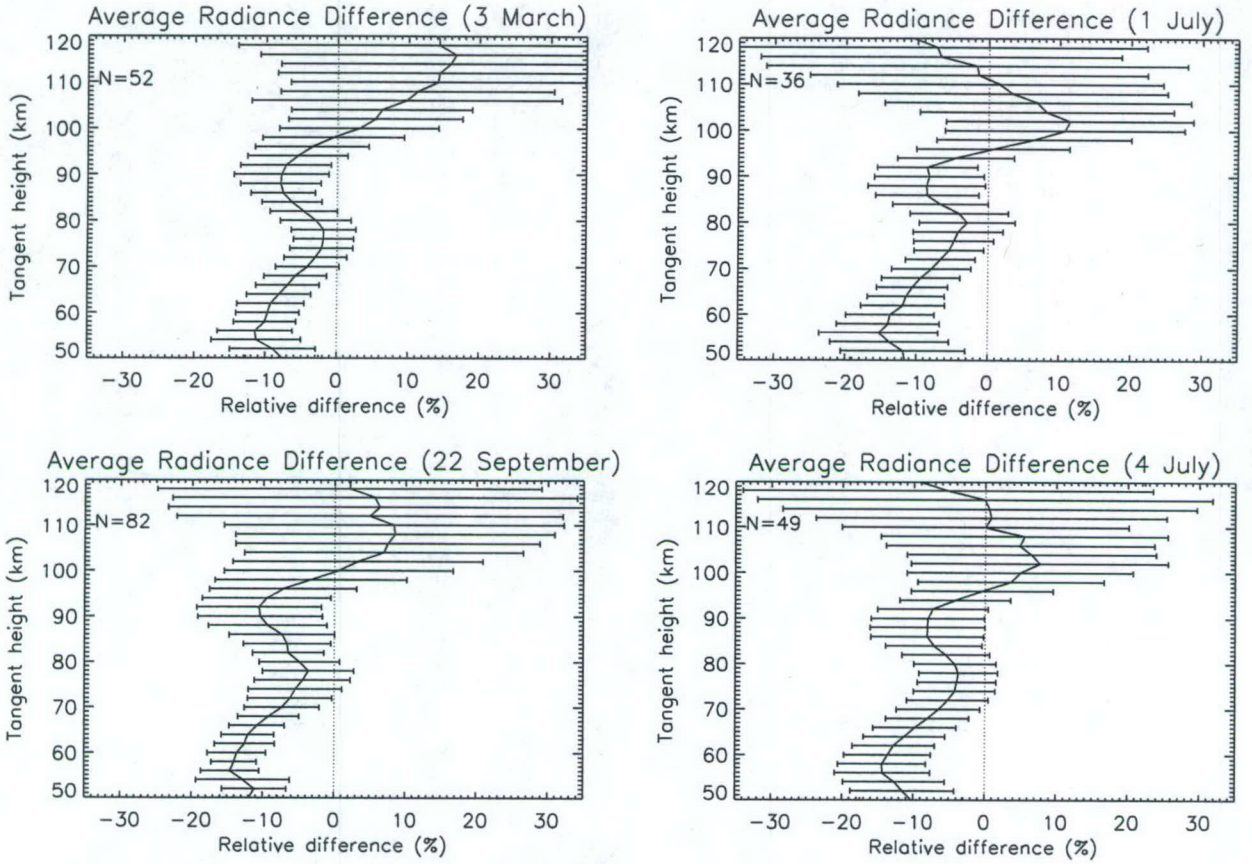

Figure 14. Panels showing the mean and the standard deviation of the residual CO_2 4.3 μm radiances, (computed-measured)/measured, for the nighttime scans of orbits (top left) 1264, 3 March; 3046, (top right) 1 July (bottom left); 4272, 22 September; and 3098, (bottom right) 4 July. N indicates the number of scans averaged.

[45] 3. The indirect contribution of OH(υ) through vibrational relaxation to N_2 and subsequent transfer to $CO_2(\upsilon_3)$ significantly enhances the CO_2 4.3 μm limb radiance in and everywhere above the upper mesosphere. However, the energy transfer estimated from the currently accepted quenching rates of OH(υ) by N_2 is not enough to explain the large SABER radiances.

[46] 4. The OH(υ) direct contribution to the SABER measurements is very small and insufficient to explain the large 4.3 μm radiance observed in the upper mesosphere.

[47] 5. Alternative mechanisms for the excitation of the $CO_2(\upsilon_3)$ levels contributing to SABER radiances have been explored and discarded.

[48] 6. An energy transfer from OH(υ) to N_2 that is more efficient than currently assumed, whereby a single $N_2(1)$ molecule is excited after the relaxation of any OH(υ) level, is required to explain the 4.3 μm radiance. On average, about 2.8–3 $N_2(1)$ molecules per OH(υ) molecule are required to explain the SABER radiances.

[49] In terms of energy transfer efficiency, this means that in every OH(υ)-N_2 collision, on average, a 30% of the OH(υ) vibrational energy needs to be transferred to $N_2(\upsilon)$. The mechanism(s) whereby the energy is transferred from OH(υ) to $N_2(\upsilon)$ is (are) still uncertain. Such a large energy transfer rate does not have, however, any impact on the currently assumed OH(υ) populations since the relaxation of OH(υ) by O_2 is considerably more efficient than the quenching by N_2.

[50] **Acknowledgments.** The IAA team was partially supported by Spanish projects PNE-017/2000-C and REN2001-3249/CLI. B. Funke has been supported through a European Community Marie Curie Fellowship. AFRL and ARCON co-authors acknowledge support from Kent Miller of the Air Force Office of Scientific Research and from the NASA SABER program. The SABER science team acknowledges support from NASA Langley under its SABER project.

References

Adler-Golden, S. (1997), Kinetic parameters for OH nightglow modeling consistent with recent laboratory measurements, *J. Geophys. Res.*, *102*, 19,969.

Alexander, J. A. F., J. T. Houghton, and W. B. McKnight (1968), Collisional relaxation from the ν_3 vibration of CO_2, *J. Phys. B At. Mol. Opt. Phys.*, *1*, 1225.

Chalamala, B. R., and R. A. Copeland (1993), Collisions dynamics of OH ($X^2\Pi$, $v = 9$), *J. Chem. Phys.*, *99*, 5807.

Dodd, J. A., S. J. Lipson, and W. A. M. Blumberg (1991), Formation and vibrational relaxation of OH ($X^2\Pi_i$, v) by O_2 and CO_2, *J. Chem. Phys.*, *95*, 5752.

García-Comas, M., M. López-Puertas, C. J. Mertens, P. P. Wintersteiner, R. H. Picard, J. R. Winick, M. G. Mlynczak, E. E. Remsberg, J. M. Russell III, and L. L. Gordley (2003), Comparisons of SABER non-LTE retrievals of kinetic temperature with ground-based measurements, *EGS Geophys. Res. Abstracts.*, *5*, 10,148.

Houghton, J. T. (1969), Absorption and emission by carbon-dioxide in the mesosphere, *Q. J. R. Meteorol. Soc.*, *95*, 1.

Kaufmann, M., O. A. Gusev, K. U. Grossmann, R. G. Roble, M. E. Hagan, C. Hartsough, and A. A. Kutepov (2002), The vertical and horizontal distribution of CO_2 densities in the upper mesosphere and lower thermosphere as measured by CRISTA, *J. Geophys. Res.*, *107*(D23), 8182, doi:10.1029/2001JD000704.

Kumer, J. B. (1991), Review of some non-LTE high altitude CO_2 4.3 μm background effects—A 10 year update, *Proc. SPIE*, *1540*, 35.

Kumer, J. B., A. T. Stair Jr., N. Wheeler, K. D. Baker, and D. J. Baker (1978), Evidence for an $OH^{\ddagger} \xrightarrow{vv} N_2^{\ddagger} \xrightarrow{vv} CO_2(\nu_3) \rightarrow CO_2 + h\nu$ (4.3 μm) mechanism for 4.3-μm airglow, *J. Geophys. Res.*, *83*, 4743.

Lacoursiere, J., M. J. Dyer, and R. A. Copeland (2003), Temperature dependence of the collisional energy transfer of $OH(\nu = 10)$ between 220 and 310 K, *J. Chem Phys.*, *118*, 1661.

López-Puertas, M. and F. W. Taylor (2001), *Non-LTE Radiative Transfer in the Atmosphere*, World Sci., Tokyo.

López-Puertas, M., G. Zaragoza, M. A. López-Valverde, and F. W. Taylor (1998a), Nonlocal thermodynamic equilibrium (LTE) atmospheric limb emission at 4.6 μm: 1. An update of the CO_2 non-LTE radiative transfer model, *J. Geophys. Res.*, *103*, 8499.

López-Puertas, M., G. Zaragoza, M. A. López-Valverde, and F. W. Taylor (1998b), Non-LTE atmospheric limb radiances at 4.6 μm as measured by UARS/ISAMS: 2. Analysis of the daytime radiances, *J. Geophys. Res.*, *103*, 8515.

López-Puertas, M., M. A. Lopez-Valverde, R. R. Garcia, and R. G. Roble (2000), A review of CO_2 and CO abundances in the middle atmosphere, in *Atmospheric Science Across the Stratopause*, *Geophys. Monogr. Ser.*, vol. 123, edited by D. E. Siskind, S. D. Eckermann, and M. E. Summers, p. 83, AGU, Washington, D. C.

Makhlouf, U. B., R. H. Picard, and J. R. Winick (1995), Photochemical-dynamical modeling of the measured response of airglow to gravity waves: 1. Basic model for OH airglow, *J. Geophys. Res.*, *100*, 11,289.

Mertens, C. J., M. G. Mlynczak, M. López-Puertas, P. P. Wintersteiner, R. H. Picard, J. R. Winick, L. L. Gordley, and J. M. Russell III (2002), Retrieval of kinetic temperature and carbon dioxide abundance from non-local thermodynamic equilibrium limb emission measurements made by the SABER experiment on the TIMED satellite, *Proc. SPIE*, *4882*, 162.

Mlynczak, M. G., and S. Solomon (1993), A detailed evaluation of the heating efficiency in the middle atmosphere, *J. Geophys. Res.*, *98*, 10,517.

Nebel, H., P. P. Wintersteiner, R. H. Picard, J. R. Winick, and R. D. Sharma (1994), CO_2 nonlocal thermodynamic equilibrium radiative excitation and infrared dayglow at 4.3 μm: Application to spectral infrared rocket experiment data, *J. Geophys. Res.*, *99*, 10,409.

Picard, R. H., J. R. Winick, R. D. Sharma, A. S. Zachor, P. J. Espy, and C. R. Harris (1987), Interpretation of infrared measurements of the high-latitude thermosphere from a rocket-borne interferometer, *Adv. Space Res.*, *10*(10), 23.

Picard, R. H., U. S. Inan, V. P. Pasko, J. R. Winick, and P. P. Wintersteiner (1997), Infrared glow above thunderstorms?, *Geophys. Res. Lett.*, *24*, 2635.

Remsberg, E., G. Lingenfelser, V. L. Harvey, W. Grose, J. Russell III, M. Mlynczak, L. Gordley, and B. T. Marshall (2003), On the verification of the quality of SABER temperature, geopotential height, and wind fields by comparison with Met Office assimilated analyses, *J. Geophys. Res.*, *108*(D20), 4628, doi:10.1029/2003JD003720.

Roble, R. G. (2000), On the feasibility of developing a global atmospheric model extending from the ground to the exosphere, in *Atmospheric Science Across the Stratopause*, *Geophys. Monogr. Ser.*, vol. 123, edited by D. E. Siskind, S. D. Eckermann, and M. E. Summers, p. 53, AGU, Washington, D. C.

Russell, J. M., III, M. G. Mlynczak, L. L. Gordley, J. Tansock, and R. Esplin (1999), An overview of the SABER experiment and preliminary calibration results, *Proc. SPIE*, *3756*, 277.

Stair, A. T., Jr., R. D. Sharma, R. M. Nadile, D. J. Baker, and W. F. Grieder (1985), Observations of limb radiance with cryogenic spectral infrared rocket experiment, *J. Geophys. Res.*, *90*, 9763.

Stiller, G. P. (Ed.) (2000), The Karlsruhe Optimized and Precise Radiative Transfer Algorithm (KOPRA), *Wissenschaft. Ber. FZKA 6487*, Forschungsz. Karlsruhe, Karlsruhe, Germany.

Winick, J. R., R. H. Picard, R. D. Sharma, R. A. Joseph, and P. P. Wintersteiner (1987), Radiative transfer effects on aurora enhanced 4.3 micron emission, *Adv. Space Res.*, *10*(10), 17.

Winick, J. R., R. H. Picard, R. D. Sharma, R. A. Joseph, and P. P. Wintersteiner (1988), 4.3 μm radiation in the aurorally dosed lower thermosphere: Modeling and analysis, in *Progress in Atmospheric Physics*, edited by R. Rodrigo et al., p. 229, Kluwer Acad., Norwell, Mass.

Wintersteiner, P. P., R. A. Joseph, and A. J. Paboojian (1990), High altitude non-equilibrium infrared emission models, *Geophys. Lab. Rep. GL-TR-90-0311*, Hanscom AFB, Mass.

Wintersteiner, P. P., A. J. Paboojian, and R. A. Joseph (1996), Studies of non-LTE atmospheric emissions: Modeling and data analysis, *Phillips Lab. Rep. PL-TR-96-2226*, Hanscom AFB, Mass.

Zaragoza, G., M. López-Puertas, M. A. López-Valverde, and F. W. Taylor (1998), The detection of the hydroxyl airglow layer in the mesosphere by ISAMS/UARS, *Geophys. Res. Lett.*, *25*, 2417.

Zaragoza, G., M. López-Puertas, and F. W. Taylor (2000), Global distribution of CO_2 in the upper mesosphere as derived from UARS/ISAMS measurements, *J. Geophys. Res.*, *105*, 19,829.

B. Funke, M. García-Comas, and M. López-Puertas, Instituto de Astrofísica de Andalucía, Apartado Postal 3004, E-18080 Granada, Spain. (puertas@iaa.es)

L. L. Gordley, GATS Inc., 11864 Canon Boulevard, Suite 101, Newport News, VA 23606, USA.

C. J. Mertens and M. G. Mlynczak, NASA Langley Research Center, Mail Stop 420, Hampton, VA 23681-2199, USA.

R. H. Picard and J. R. Winick, Air Force Research Laboratory, Space Vehicles Directorate, 29 Randolph Road, Hanscom AFB, MA 01731-3010, USA.

J. M. Russell III, Center for Atmospheric Sciences, Hampton University, 23 Tyler Street, Hampton, VA 23668, USA.

P. P. Wintersteiner, ARCON Corporation, 260 Bear Hill Road, Waltham, MA 02154, USA.